Electronic Supplementary Material (ESI) for Chemical Science.
This journal is © The Royal Society of Chemistry 2023

Supporting Information

Ru/RuO_2 Heterostructure Boosting Electrochemistry-Assisted Selective Benzoic Acid Hydrogenation

Zifan Cao [a], Chenhui Wang [a], Yifan Sun [a], Menghui Liu [a], Wei Li [a], Jinli Zhang [a,b], Yan Fu [a*]*

a. School of Chemical Engineering and Technology, Tianjin University, Tianjin, 300350, China

b. School of Chemistry and Chemical Engineering, Shihezi University, Shihezi, 832003, China

* Corresponding author

E-mail: fuyan@tju.edu.cn; zhangjinli@tju.edu.cn

Materials and methods

Materials and reagents

Ruthenium (III) chloride trihydrate ($RuCl_3 \cdot 3H_2O$) and 1-cyclohexene-1-carboxylic acid (CEA) were obtained from Meryer Chemical Technology Co., Ltd. (Shanghai). Cyclohexanecarboxylic acid (CCA) was purchased from Yuanye Biotechnology Co., Ltd. 4-Methyl cyclohexane carboxylic acid and *p*-methyl benzoic acid were purchased from Tianjin Heowns Co., Ltd. (Tianjin). Sodium sulphate (Na_2SO_4) and benzoic acid (BA) were purchased from Bide Pharmatech Ltd. Potassium hydroxide (KOH) (90%) was purchased from Macklin Biochemical Co., Ltd. (Shanghai). H_2SO_4 (95~98 wt%) was obtained from Fengchuan Chemical Reagent Co., Ltd. (Tianjin). Nafion 117 membrane was purchased from Jingchong Electronic Technology Development Co., Ltd. (Shanghai). Carbon cloth (CC) was obtained from Phychemi (Wuhan, China). Silver chloride electrode (Ag/AgCl) and platinum plate electrode were purchased from Incole Union Technology Co., Ltd. (Tianjin).

Synthesis procedure of electrode materials

CC was cut into pieces of 10 mm×30 mm, then treated for 48 h with nitric acid (68 wt%) at room temperature. Cyclic voltammetry (CV) was applied to prepare Ru-based electrodes with a three-electrode cell. An Ag/AgCl electrode (saturated with KCl) was selected as the reference electrode. Both working and counter electrodes were CC, of which the dimensions were 3 cm×1.5 cm and 3.5 cm×2.5 cm respectively.

In a typical synthesis, 2.13 g of Na_2SO_4 and 30 mg of $RuCl_3$ were dissolved in 30 mL of H_2O. After sufficiently mixing, the resulting solution was used for subsequent electrodeposition. 100

cycles of CV electrodeposition were carried out between -0.8 and 1.1 V at a scanning rate of 0.1 V s^{-1}. Then the working electrode was rinsed with distilled water and ethyl alcohol, and dried at room temperature. For comparison, the control electrodes were prepared with other potential ranges.

Characterizations

The morphologies were characterized by Apreo S LoVac field emission scanning electron microscope (FESEM), and the lattice fringes were analyzed using TEM (JEM-F200, Japan). The valence states were tested by Thermo Scientific ESCALAB 250Xi Spectrometer X-ray photoelectron spectroscopy (XPS). Products after ECH were determined by gas chromatography (GC, Agilent 7820 A) equipped with an HP-5 column (30 m × 320 μm × 0.25 μm). *In-situ* Raman spectroscopic studies were conducted on a laser confocal Raman microscopy (LabRAM HR Evolution). The concentrations of Ru were tested by ICP-OES (PerkinElmer 8300). Gas chromatography–mass spectrometry (GC-MS, Agilent 7890A GC-5975C MS) was carried out to verify the products.

Electrochemical measurements

Electrochemical measurements were carried out by CHI760E workstation in a three-electrode system. The Hg/HgO electrode, as-prepared Ru/CC electrode and Pt plate electrode were adopted as the reference, working and counter electrodes, respectively. All the potentials were measured based on a Hg/HgO reference (1 M KOH) and converted to reversible hydrogen electrode scale according to the following equation:

$$E_{(RHE)} = E_{(Hg/HgO)} + 0.098 + 0.059pH$$

Cyclic voltammetry was conducted from -1.065 to 0.335 V versus Hg/HgO at a scanning rate of 100 mV s^{-1}. Before linear scan voltammogram (LSV), the interference of solution resistance was removed with iR-correction (85%). LSV profiles were acquired at a scanning rate of 5 mVs^{-1}. Electrochemical impedance spectroscopy (EIS) was completed at an initial voltage of -1.365 V with a frequency range from 10^5 to 0.1 Hz.

Electrocatalytic hydrogenation of BA

ECH of BA was performed in a H-type electrolyzer. Nafion 117 was used as the membrane and placed between the cathode and anode chambers. The as-synthesized Ru-based electrode was employed as the cathode with a geometric surface area of 3 cm^2, which was immersed in 20 mL of 0.1 M KOH. The Pt plate was used as the anode, which was immersed in 20 mL of 0.05 M H_2SO_4. Unless otherwise mentioned, ECH was conducted by a galvanostatic method with 50 mM BA added. The applied current during ECH of BA was fixed at 200 mA. After ECH, 200 μL of the cathodic electrolyte was neutralized with 200 μL of 0.5 M H_2SO_4. Then the above solution was extracted with 200 μL of ethyl acetate. The reactants and products were quantitatively analyzed by gas chromatography. The Agilent HP-5 GC column was adopted at the column temperature of 130.0 ℃. The injector temperature was 260.0 ℃, the pressure was 27.7 psi and the N_2 flow rate was 48.2 mL/min with no split ratio. The detector temperature was set at 270.0 ℃ and the flow rate of make-up gas was 25.0 mL/min.

The conversion of BA, the selectivity of CCA and CEA, as well as the Faradaic efficiency were calculated as follows:

$$\text{BA}_{\text{conversion}} = \frac{\text{BA consumed moles}}{\text{BA initial moles}} \quad (1)$$

$$\text{CCA}_{\text{selectivity}} = \frac{\text{CCA formed moles}}{\text{BA consumed moles}} \quad (2)$$

$$\text{CEA}_{\text{selectivity}} = \frac{\text{CEA formed moles}}{\text{BA consumed moles}} \quad (3)$$

$$FE_{ECH} = \frac{\sum(z_i \times n_i \times F)}{Q_{total}} \quad (4)$$

$$Q = It \quad (5)$$

where z is the number of electrons obtained by the conversion of BA to CCA (z = 6) and CEA (z=4), i is per product, F is the Faraday constant (96485C mol^{-1}), I is the value of constant current applied during ECH and t is the time of constant current applied during ECH.

Density functional theory (DFT) calculations

Vienna ab initio simulation package (VASP) was used to conduct spin polarized DFT calculations. Projector-augmented wave (PAW) method and Perdew–Burke–Ernzerhof (PBE) functional were used to describe the ionic cores and exchange-correlation energies, respectively. The cut-off energy for the plane-wave basis was 450 eV. The computational structure consists of a periodic P (3 × 2) RuO_2 (210) structure and a periodic P (2 × 7) Ru (101) structure, which are matched with an error of less than 5%. To avoid interactions in the z-direction, the vacuum gap in the z-axis direction between the periodic images was set to 15 Å. For computing the adsorption energies of potassium benzoate, potassium cyclohexene carboxylate and potassium cyclohexane carboxylate, the convergence of force and energy were set to 1×10^{-5} eV and 0.05 eV·$Å^{-1}$ respectively. Brillouin zone integration was sampled with a 2×2×1 Monkhorst-Pack k-point mesh. The adsorption energies of potassium benzoate, potassium cyclohexene carboxylate and potassium cyclohexane carboxylate on Ru (101), RuO_2 (210) and Ru/RuO_2 interfaces were calculated by the

following equations:

$$\Delta E_{X*}=E_{(surface+X*)}-(E_{surface}+E_{X*}) \quad (4)$$

where X represents potassium benzoate, potassium cyclohexene carboxylate or potassium cyclohexane carboxylate. $E_{(surface+X*)}$ means the energy of substrate with an adsorbed X molecule. $E_{surface}$ denotes the energy of bare substrate. E_{X*} is the energy of molecule X.

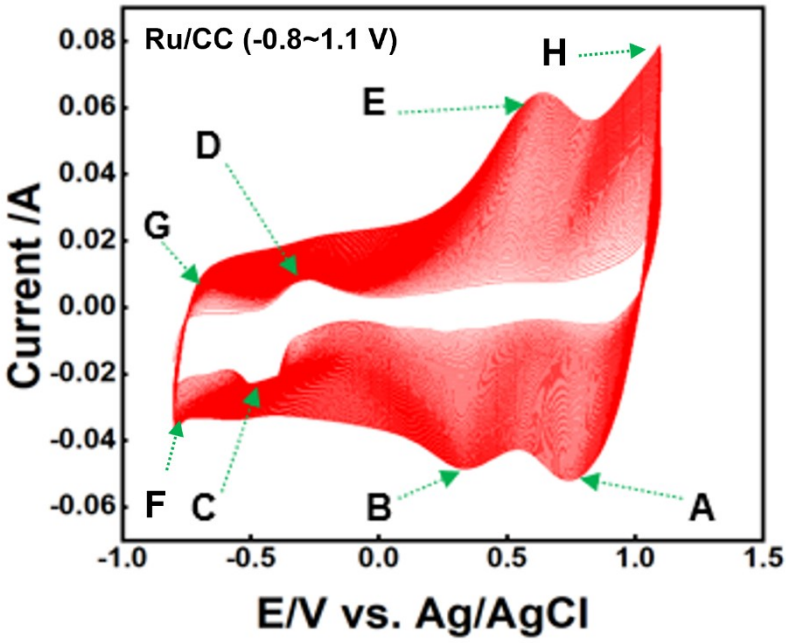

Fig. S1 CV profiles collected during electrodeposition process of Ru/CC (-0.8-1.1 V).

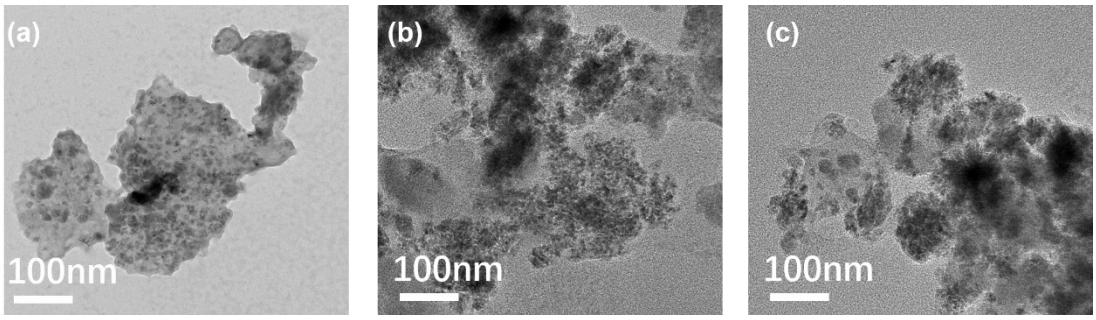

Fig. S2 TEM images of (a) Ru/CC (-0.8~1.1 V), (b) Ru/CC (-0.8~0 V), (c) Ru/CC (0~1.1 V).

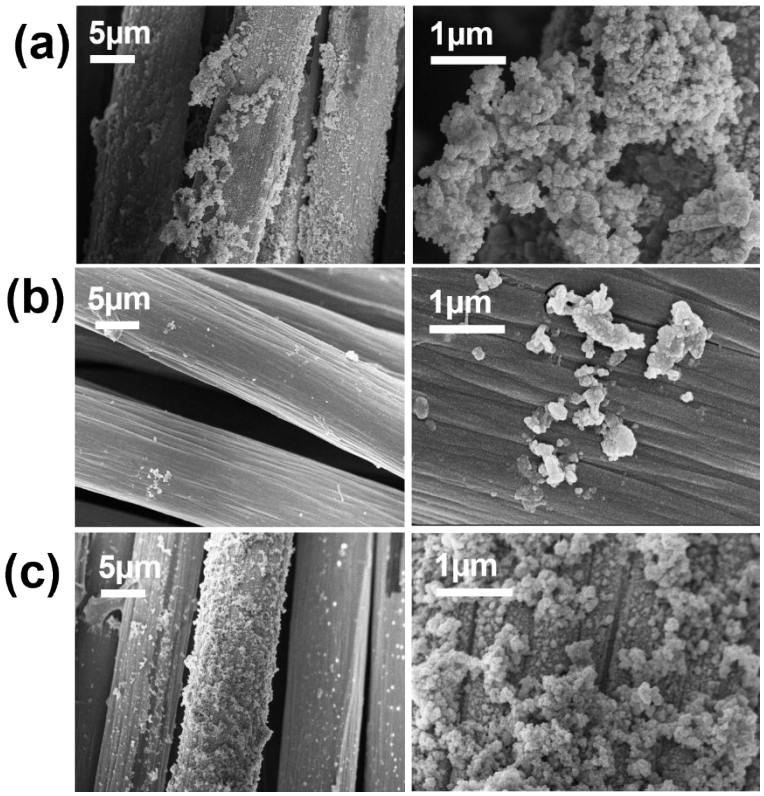

Fig. S3 SEM images of (a) Ru/CC (-1.0~0.9 V), (b) Ru/CC (-0.3~1.6 V), (c) Ru/CC (-1.3~0.6 V).

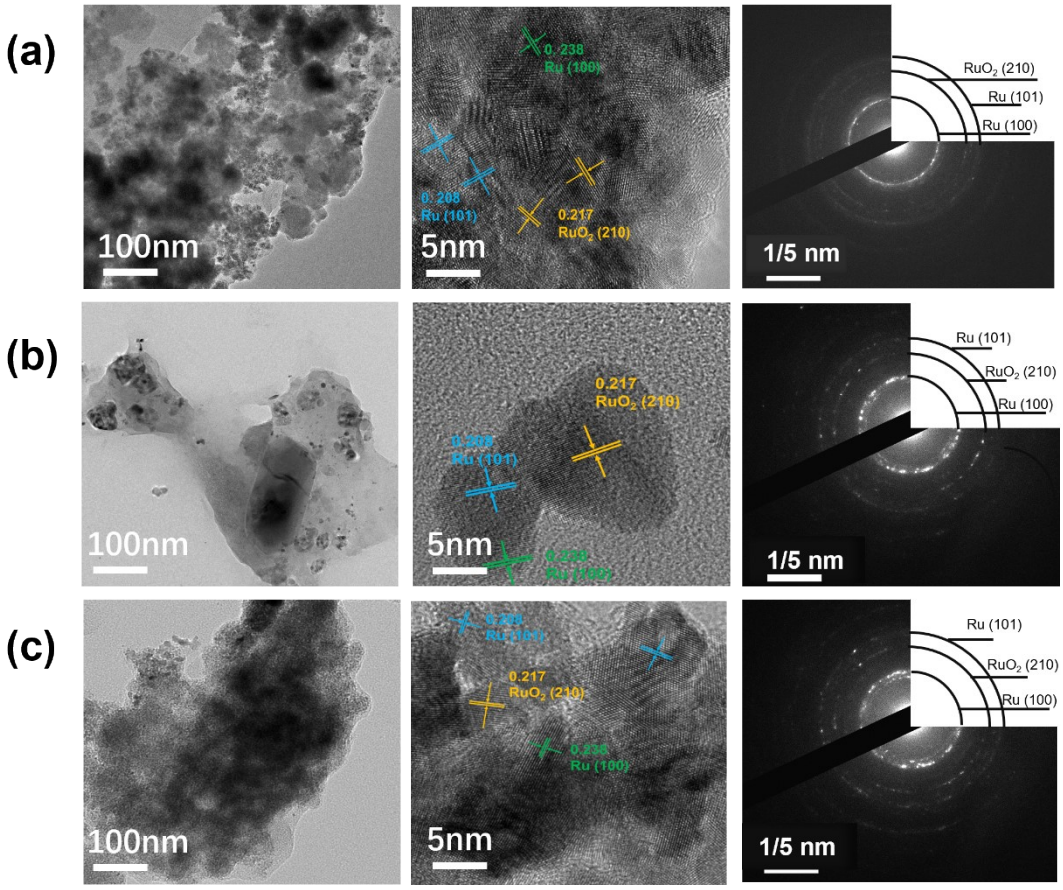

Fig. S4 TEM, HRTEM images and corresponding SAED patterns of (a) Ru/CC (-1.0~0.9 V), (b) Ru/CC (-0.3~1.6 V), (c) Ru/CC (-1.3~0.6 V).

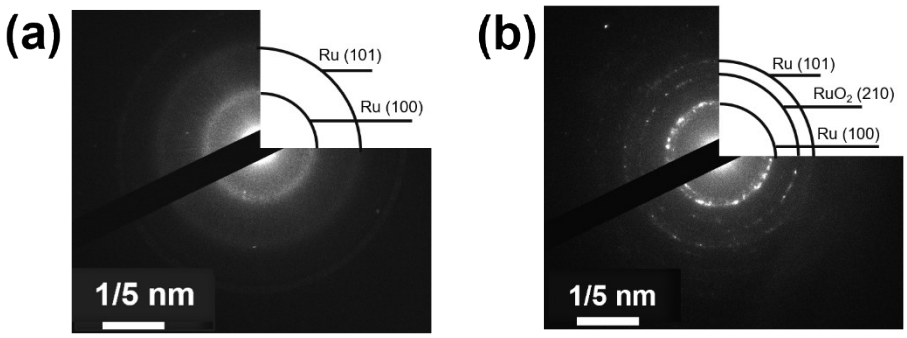

Fig. S5 SAED patterns of (a) Ru/CC (-0.8~0 V) and (b) Ru/CC (0~1.1 V).

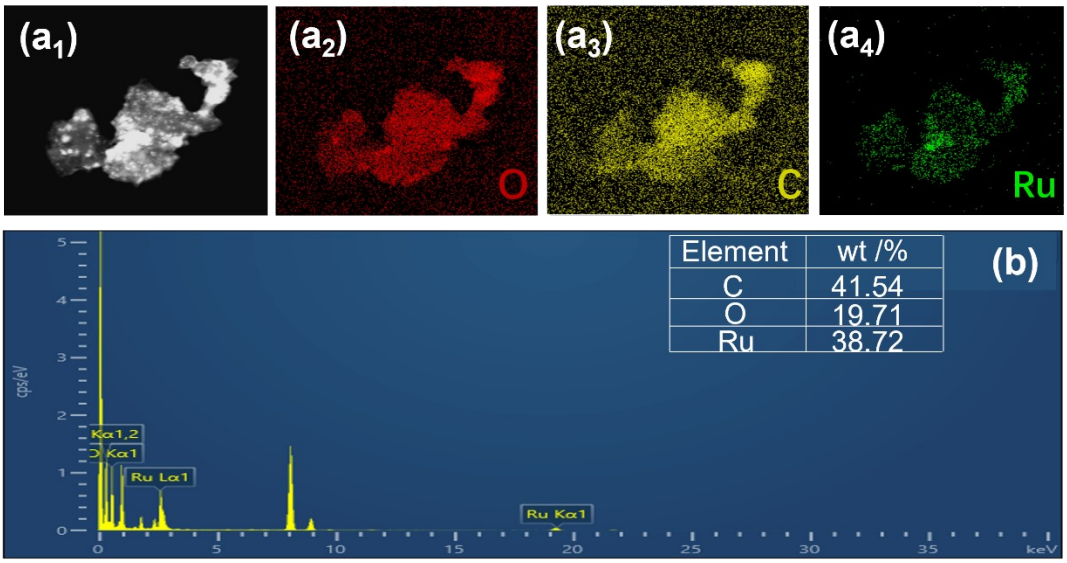

Fig. S6 HAADF-STEM and elemental mapping for Ru/CC (-0.8~1.1 V).

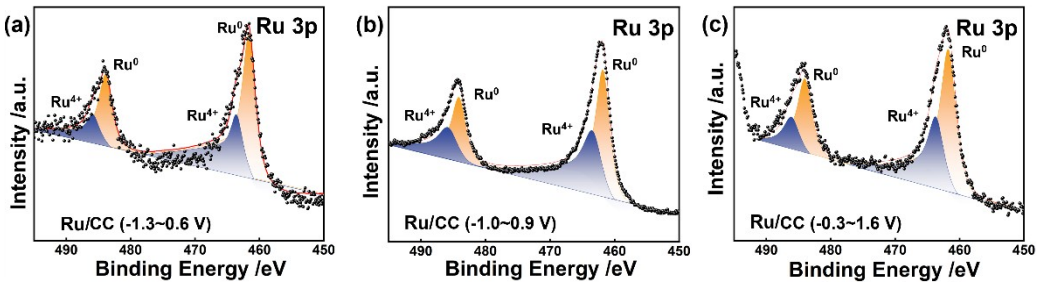

Fig. S7 High-resolution XPS spectra of Ru 3p for (a) Ru/CC (-1.3~0.6 V), (b) Ru/CC (-1.0~0.9 V), (c) Ru/CC (-0.3~1.6 V).

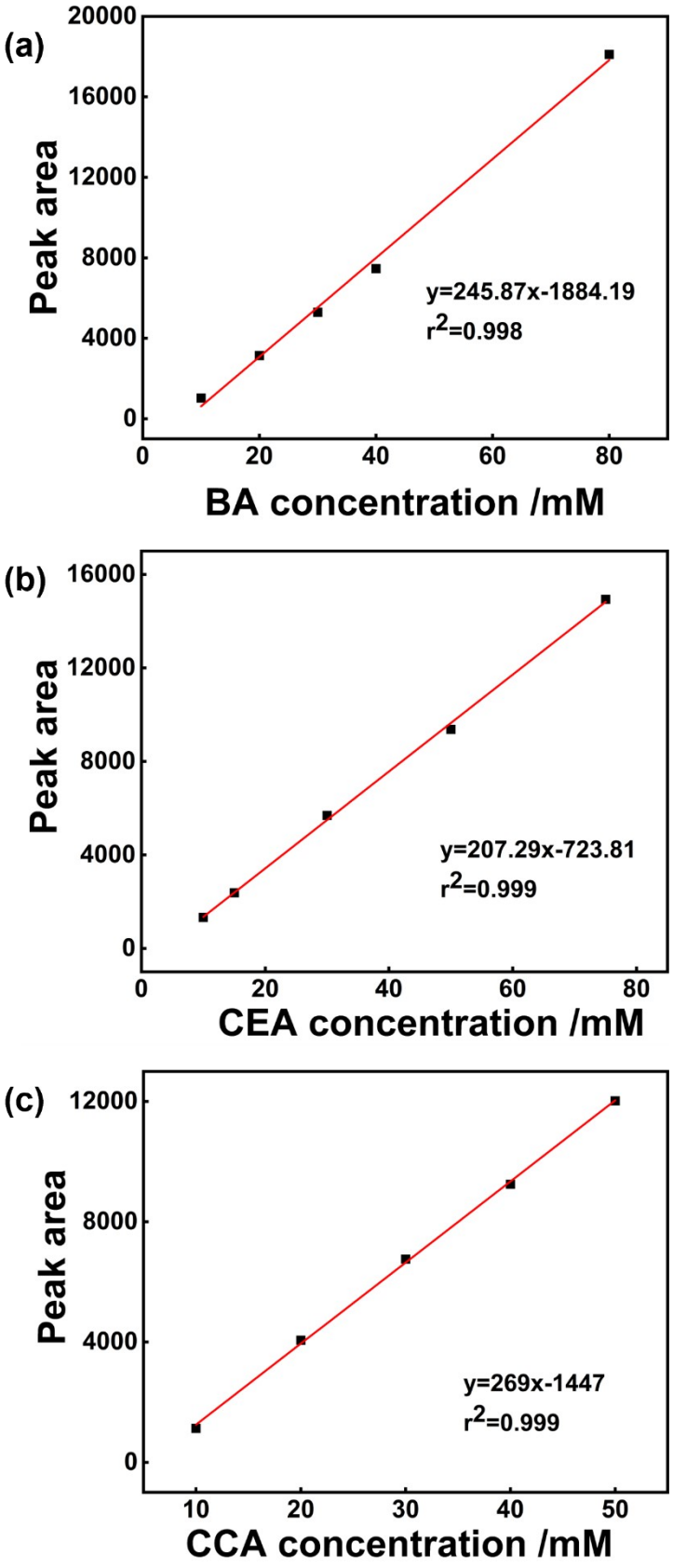

Fig. S8 Standard curves for (a) BA, (b) CEA and (c) CCA.

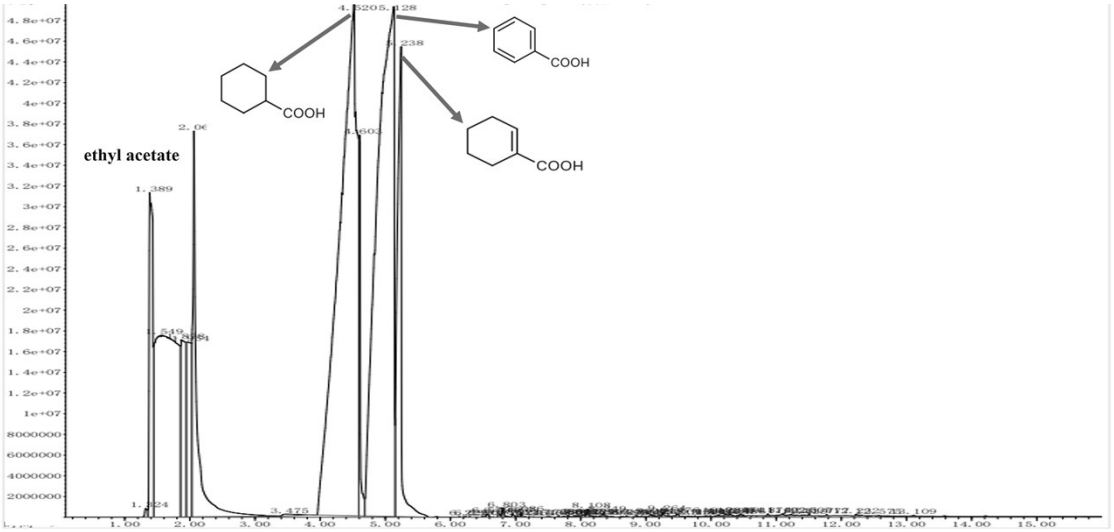

Fig. S9 GC-MS full spectrum of the catholyte after 30 min of reaction and library search report.

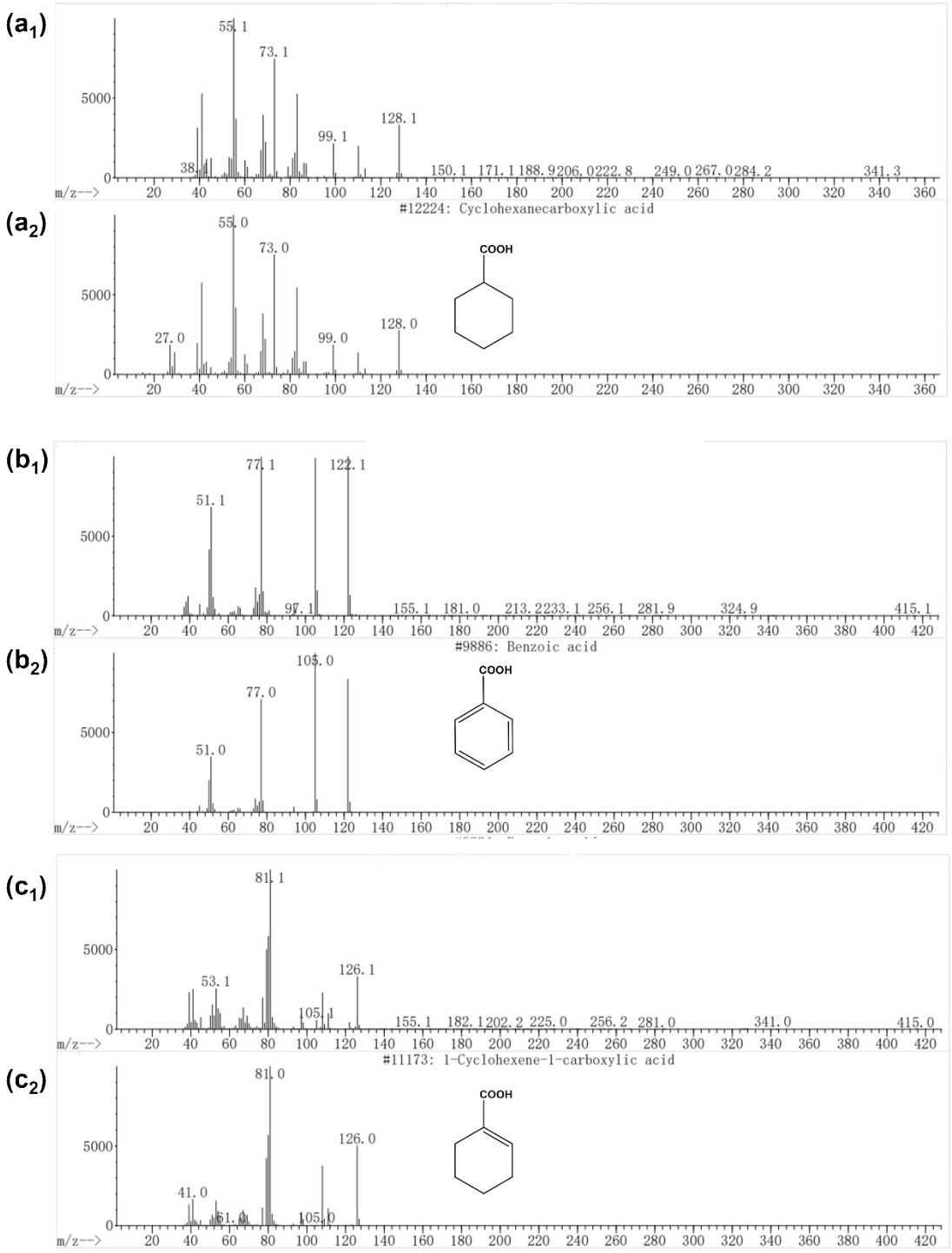

Fig. S10 The results of GC-MS: (a_1, a_2) the spectrum after ECH and the standard spectrograms of CCA, (b_1, b_2) the spectrum after ECH and the standard spectrograms of BA, (c_1, c_2) the spectrum after ECH and the standard spectrograms of CEA. Operating conditions: BA: 50 mM, KOH: 0.1 M, Current density: 200/3 mA·cm^{-2}, RT: 30 min.

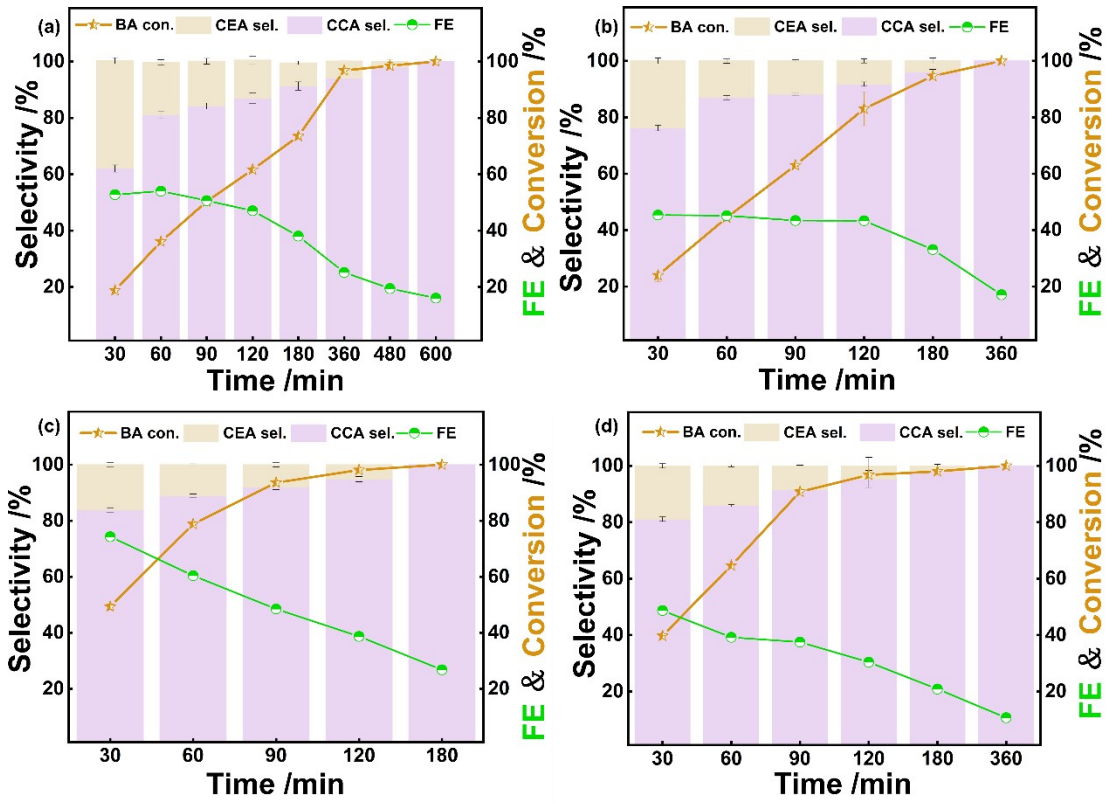

Fig. S11 The conversion, FE and selectivity during ECH of 50 mM BA over Ru/CC (-0.8~1.1 V) in 0.1 M KOH at different current densities: (a) 100/3 mA cm^{-2}; (b) 150/3 mA cm^{-2}; (c) 200/3 mA cm^{-2}; (d) 250/3 mA cm^{-2}.

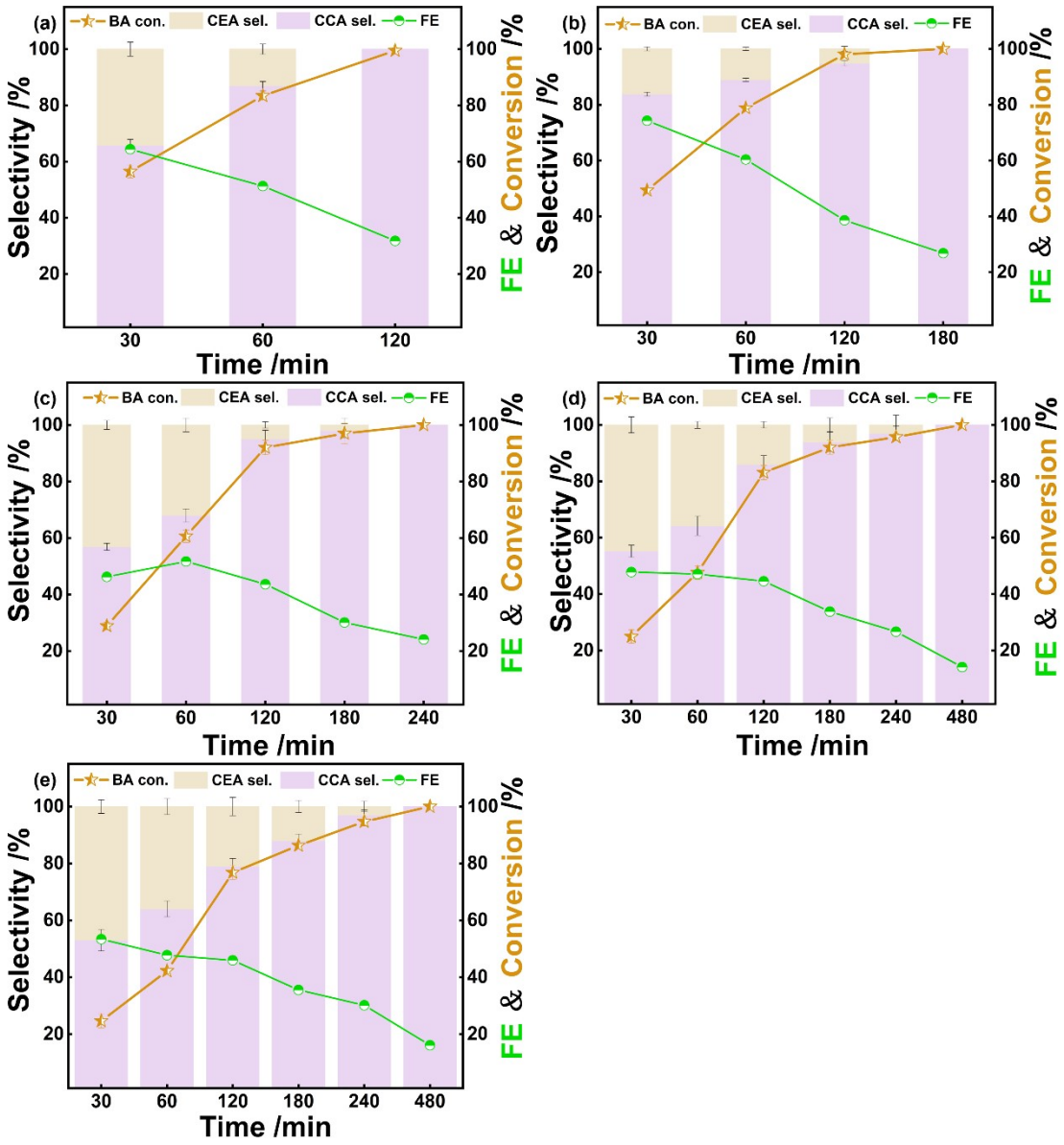

Fig. S12 The conversion, FE and selectivity over Ru/CC (-0.8~1.1 V) in 0.1 M KOH at 200/3 mA cm^{-2}: (a) 40 mM; (b) 50 mM; (c) 60 mM; (d) 70 mM; (e) 80 mM BA.

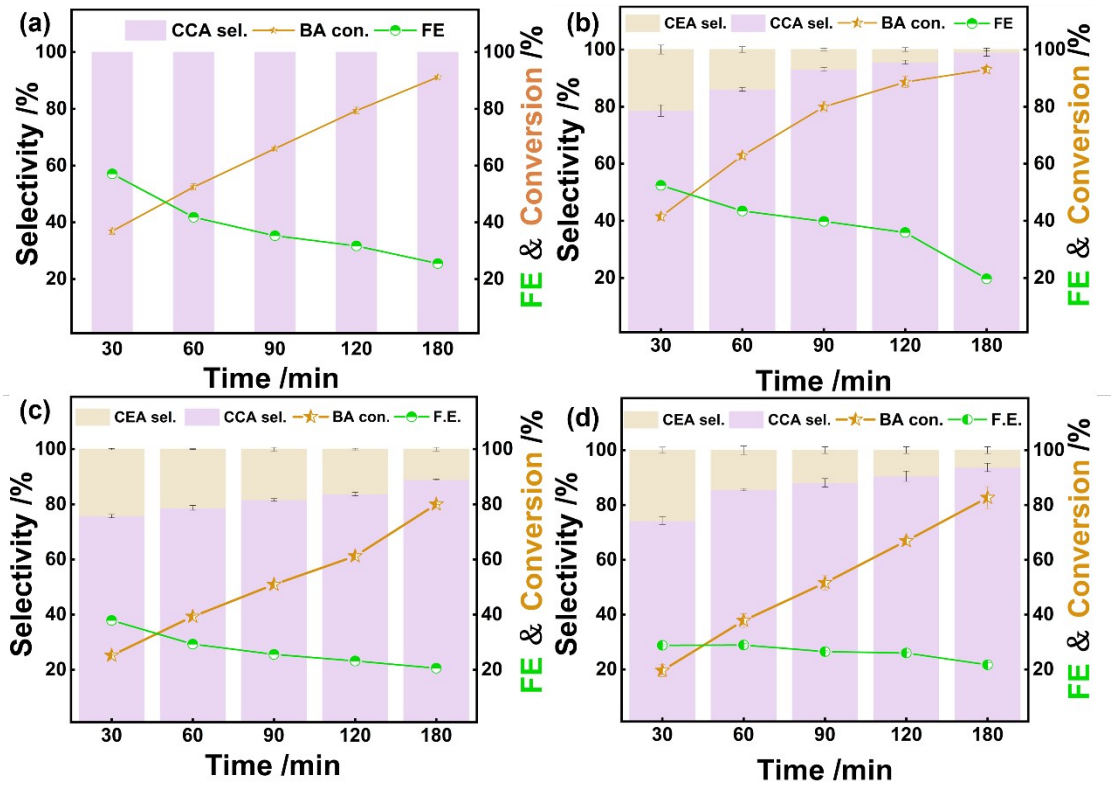

Fig. S13. (a) The conversion, selectivity and FE over Ru/CC (-0.8~1.1 V) during ECH of 5 mM BA at 20/3 mA cm^{-2} in 0.05 M H_2SO_4. The conversion, selectivity and FE over Ru/CC (-0.8~1.1 V) during ECH of 50 mM BA at 200/3 mA cm^{-2} in (b) 0.1 M NaOH, (c) 0.1 M Na_2CO_3, (d) 0.1 M $NaHCO_3$.

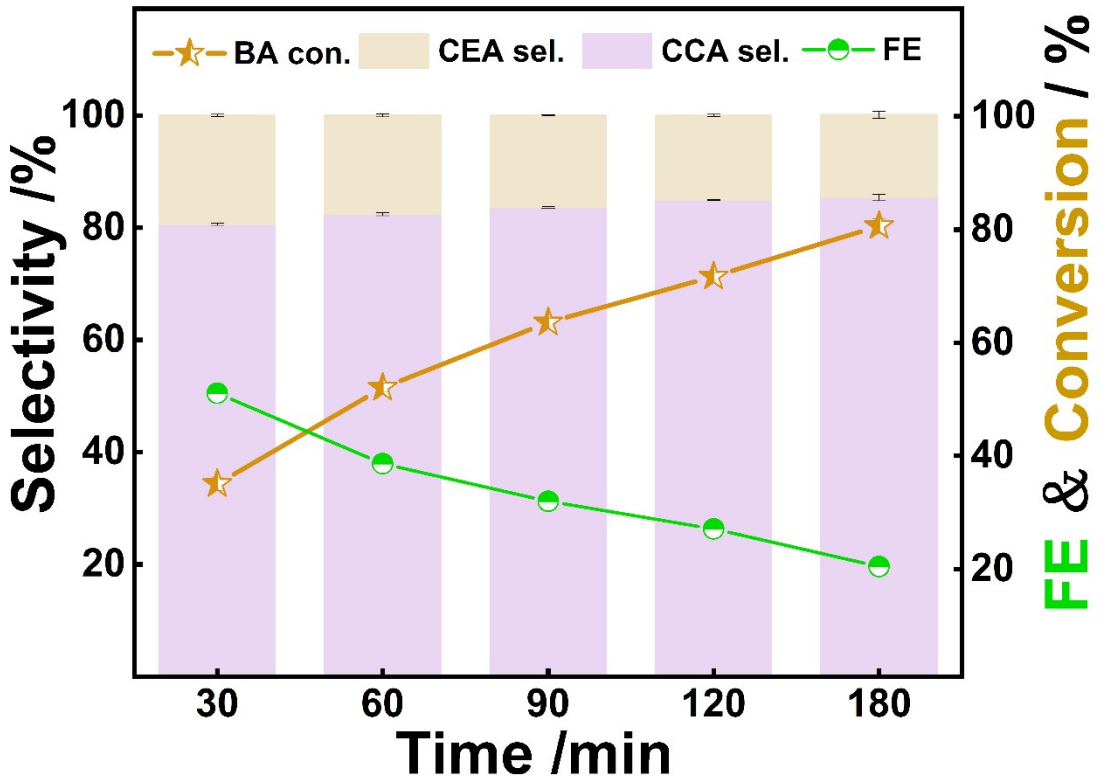

Fig. S14 The conversion, FE and selectivity during ECH of 50 mM BA at 200/3 mA cm^{-2} over Ru/CC (-0.8~0 V) prepared with 225 CV cycles.

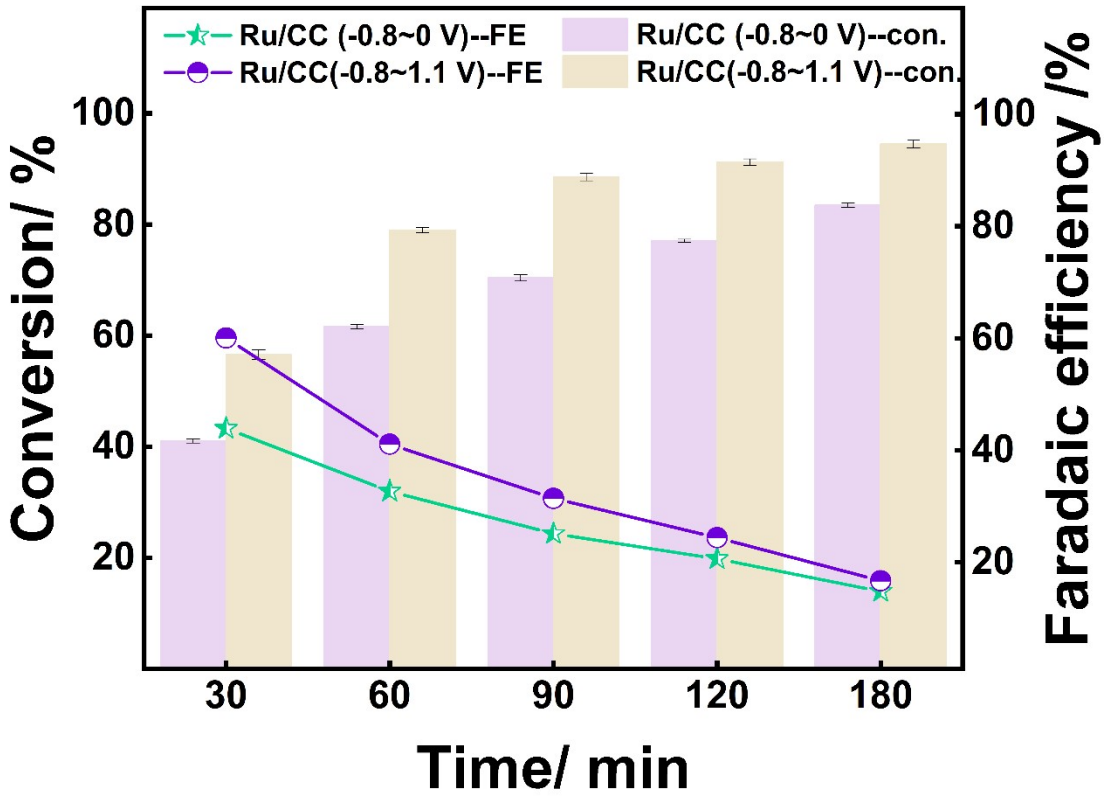

Fig. S15 ECH of 50 mM CEA at 200/3 mA cm^{-2} over Ru/CC (-0.8~1.1 V) with 100 CV cycles and Ru/CC (-0.8~0 V) with 225 CV cycles.

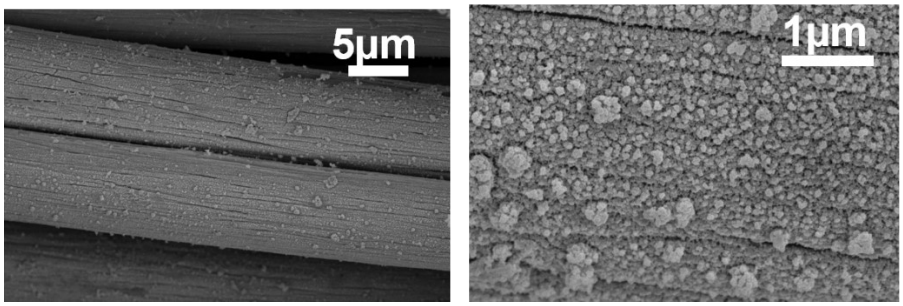

Fig. S16 SEM images of spent Ru/CC (-0.8~1.1 V) after 7 ECH cycles.

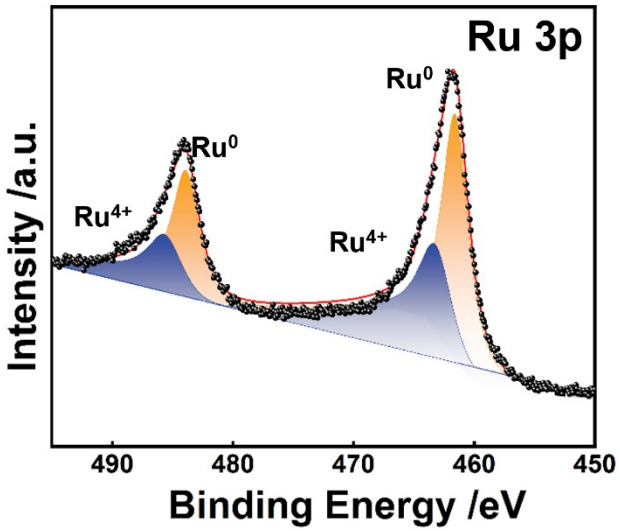

Fig. S17 High-resolution XPS spectra of Ru 3p for spent Ru/CC (-0.8~1.1 V) after 7 ECH cycles.

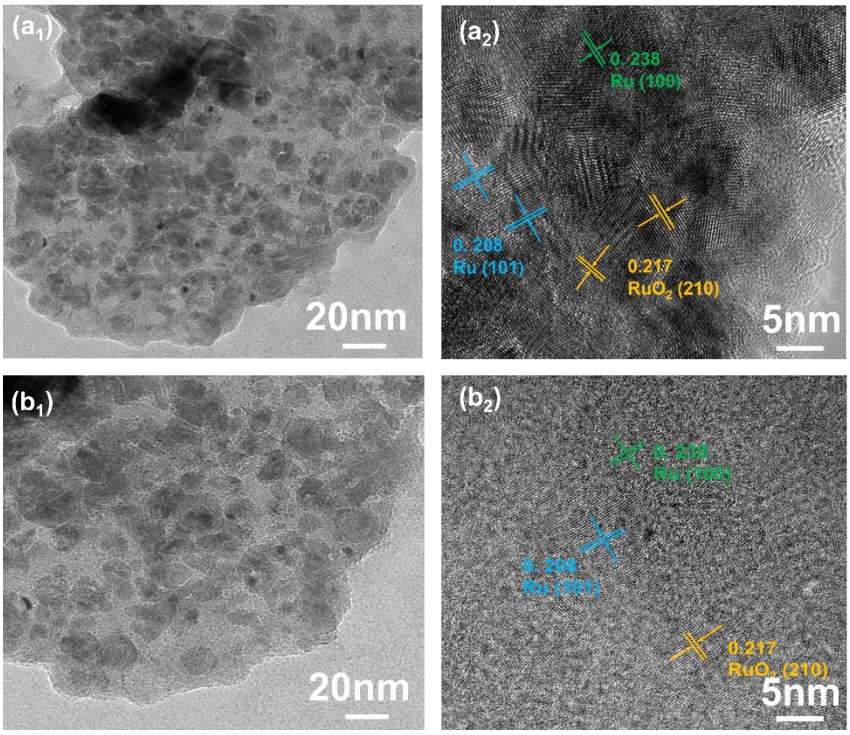

Fig. S18 (a_1, b_1) TEM and (a_2, b_2) HRTEM images of Ru/CC (-0.8~1.1 V) (a: Before ECH; b: After ECH).

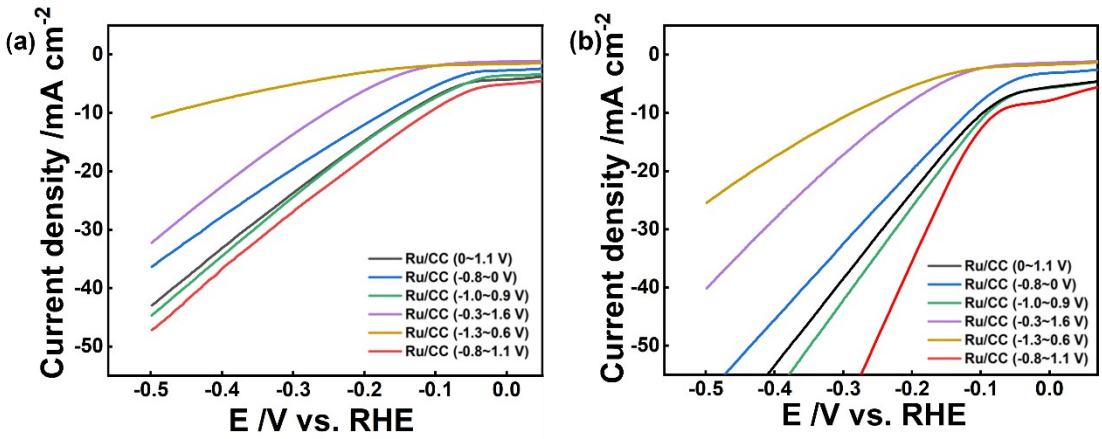

Fig. S19 LSV profiles of Ru/CC (-0.8~1.1 V), Ru/CC (-0.8~0 V), Ru/CC (0~1.1 V), Ru/CC (-1.0~0.9 V), Ru/CC (-1.3~0.6 V) and Ru/CC (-0.3~1.6 V) in 0.1 M KOH solution (a) with and (b) without 50 mM BA.

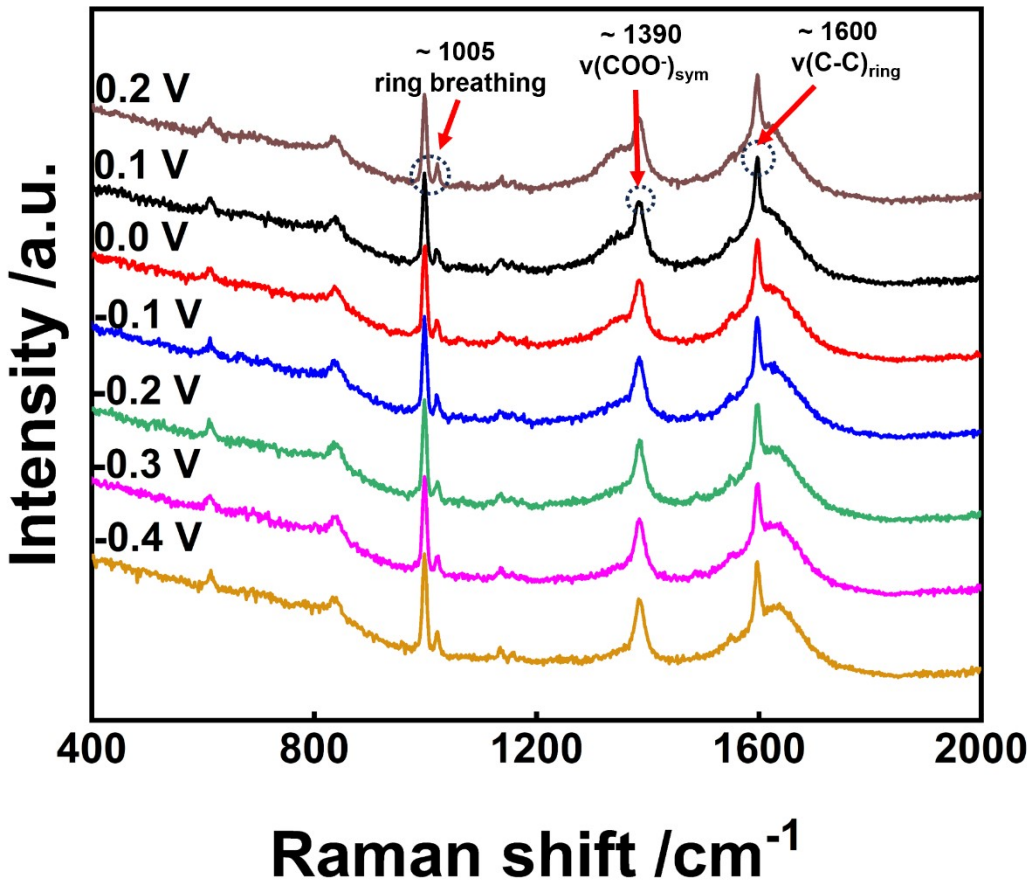

Fig. S20 In situ Raman spectra collected on carbon cloth for benzoate in KOH solution.

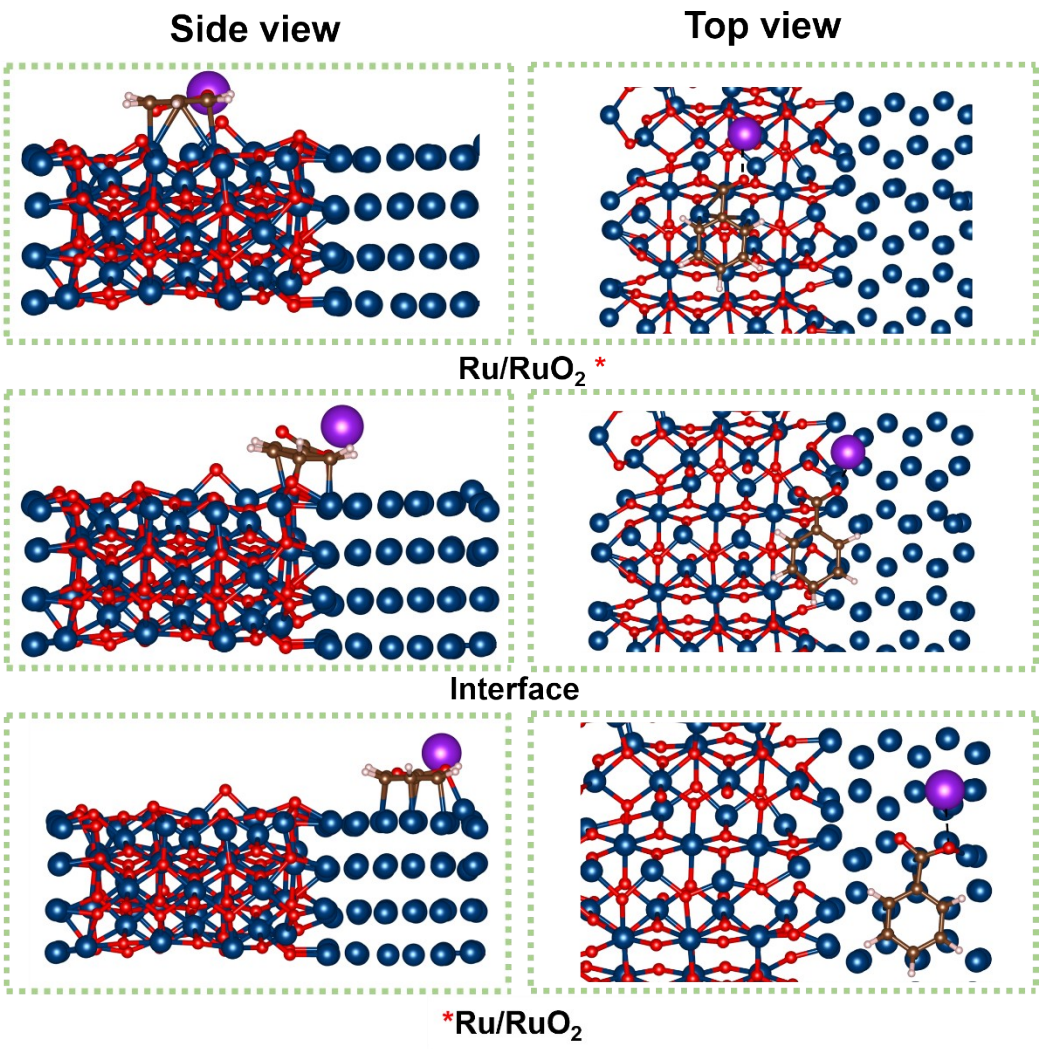

Fig. S21 Various calculated potassium benzoate adsorption sites on Ru/RuO_2*, interface and *Ru/RuO_2, showing side view (left) and top view (right) of each structure.

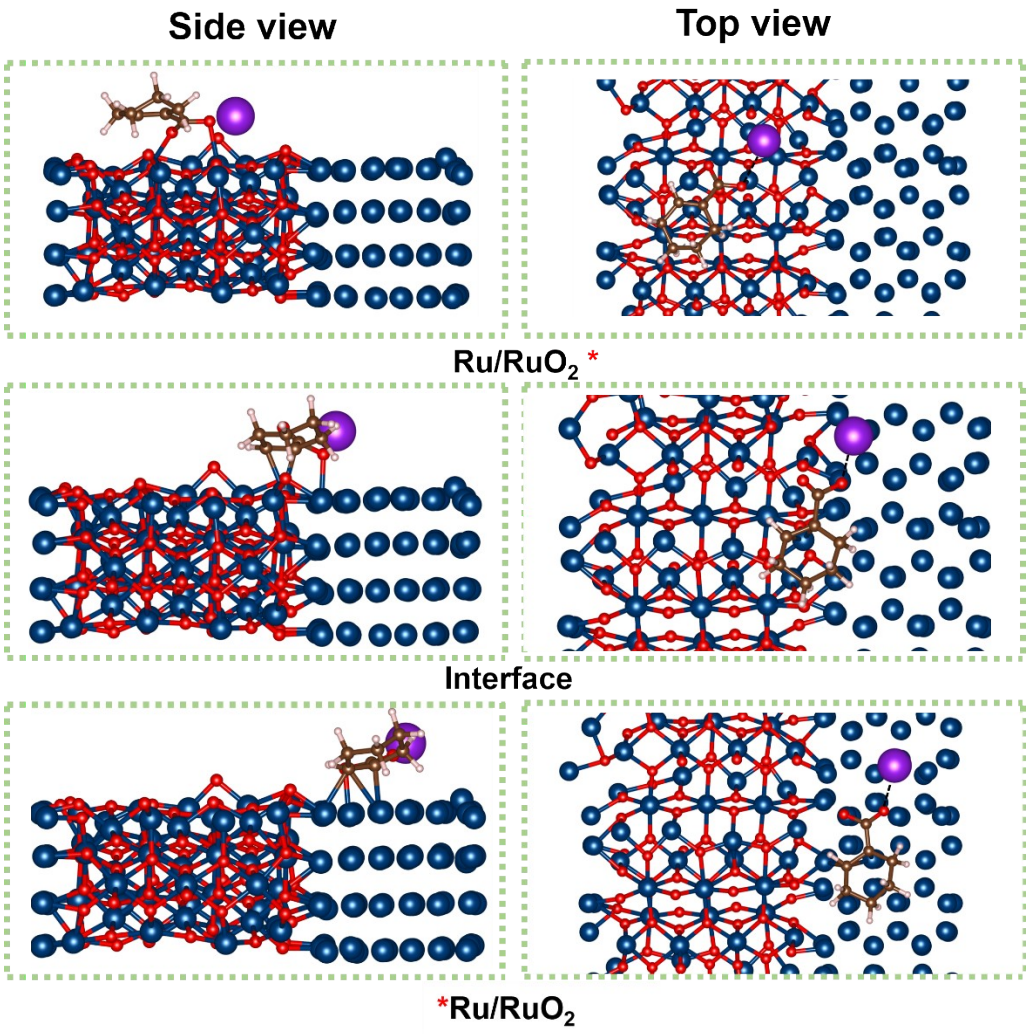

Fig. S22 Various calculated potassium cyclohexene carboxylate adsorption sites on Ru/RuO_2*, interface and *Ru/RuO_2, showing side view (left) and top view (right) of each structure.

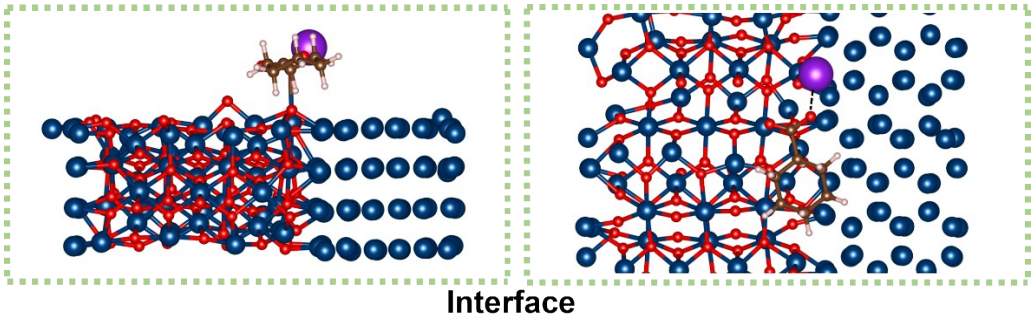

Fig. S23 Calculated potassium cyclohexane carboxylate adsorption sites on the interface, showing side view (left) and top view (right).

Table S1. Summary of catalysts for BA hydrogenation.

Catalysts	Method	Solvent	Time (h)	Temperature (K)	Pressure (MPa)	Con. (% BA)	Sel. (% CCA)
$Rh/NaNbO_3$[1]	TCH	water	5	RT	0.5	100	100
$NiZrB/Al_2O_3$[2]	TCH	cyclohexane	4	425	5.0	99.9	95.3
Ni/Al_2O_3-NS[3]	TCH	cyclohexane	2.5	423	1.0	99	98
Ru/NPCNs[4]	TCH	water	1.5	353	1.0	74.2	99
Ru/PPh_3@FDU[5]	TCH	water	8	373	2.0	99	98
Pt/TiO_2[6]	TCH	*n*-hexane	1	353	5.0	90	99
RhPt/MCM-41[7]	TCH	hexane	0.33	313	1.0	99	99
Ru/C-TiO_2[8]	TCH	water	2	343	2.5	99.5	86
Ru–MC-g[9]	TCH	water	2	393	4.0	93.7	99.1
Pd@CN[10]	TCH	water	24	358	0.1	50	100
Rh-PVP[11]	TCH	water	1	423	1.0	99	96
$Ni_2Mg_{0.5}Al_1$-MMO[12]	TCH	cyclohexane	3	423	5.0	98.39	98.49
Ni/CSC-b[13]	TCH	THF	8	473	3.0	86.2	100
$PtRu/Ni(OH)_2$[14]	ECH	H_2SO_4	1.5	RT	AP	100	100
$Pt_1Ru_{1.5}$[15]	ECH	/	2	RT	AP	/	/
PtRu/CP-4[26]	ECH	H_2SO_4	2.5	RT	AP	100	100

Table S2. The valence states and binding energies (B.E.s) of Ru 3p as well as the percentages of metallic Ru^0 species

Electrodes	Ru^0		Ru^{4+}		Ru^0
	B.E. (eV) $3p_{3/2}$	B.E. (eV) $3p_{1/2}$	B.E. (eV) $3p_{3/2}$	B.E. (eV) $3p_{1/2}$	content (%)
Ru/CC (-0.8~1.1 V)	461.88	484.08	464.38	486.48	68.13
Ru/CC (-0.8~0 V)	461.58	483.88	/	/	100
Ru/CC (0~1.1 V)	461.88	484.18	463.58	485.88	64.26
Ru/CC (-1.0~0.9 V)	461.74	483.98	463.68	486.05	71.75
Ru/CC (-1.3~0.6 V)	461.88	484.18	463.58	486.18	79.55
Ru/CC (-0.3~1.6 V)	461.65	483.97	463.77	486.25	66.22
Spent Ru/CC (-0.8~1.1 V)	461.78	484.18	463.28	485.58	63.50

Table S3. The ECH performance in different electrolytes.

	Electrolyte concentration/ M	Current density/ mA cm^{-2}	BA concentration/ mM	Reaction time/ min	BA conversion / %	CCA selectivity /%
H_2SO_4	0.05	20	5	180	91.67	100
NaOH	0.1	200	50	180	93.30	95.65
Na_2CO_3	0.1	200	50	180	80.05	88.94
$NaHCO_3$	0.1	200	50	180	82.75	93.72

Table S4. Overpotentials (mV) for different catalysts in the absence and presence of 50 mM BA in 0.1 M KOH.

Electrodes	Overpotential (10 mA cm^{-2}) /mV	
	With BA	Without BA
Ru/CC (-0.8~1.1 V)	110	90
Ru/CC (-0.8~0 V)	172	112
Ru/CC (0~1.1 V)	141	119
Ru/CC (-1.0~0.9 V)	138	97
Ru/CC (-1.3~0.6 V)	475	288
Ru/CC (-0.3~1.6 V)	255	225

References

[1] Y. Hu, W. Chen, Highly Efective $Rh/NaNbO_3$ Catalyst for the Selective Hydrogenation of Benzoic Acid to Cyclohexane Carboxylic Acid Under Mild Conditions, Catal. Lett., 2022, 152, 2164–2177.

[2] X. Wen, Y. Cao, Significant effect of base on the improvement of selectivity in the hydrogenation of benzoic acid over NiZrB amorphous alloy supported on γ-Al_2O_3, Catal. Sci. Technol., 2015, 5, 3281.

[3] W. Lian, B. Chen, Acquiring Clean and Highly Dispersed Nickel Particles (ca. 2.8 nm) by Growing Nickel-Based Nanosheets on Al_2O_3 as Efficient and Stable Catalysts for Harvesting Cyclohexane Carboxylic Acid from the Hydrogenation of Benzoic Acid, Ind. Eng. Chem. Res., 2019, 58, 2846–2856.

[4] Z. Qiu, S. Ma, Nitrogen-Doped Porous Two-dimensional Carbon Nanosheets Derived from ZIF-8 as Multifunctional Supports of Ru Nanoparticles for Hydrogenation of Benzoic Acid, Catal. Lett., 2023, 153, 388–397.

[5] X. Ren, M. Guo, Microenvironment Engineering of Ruthenium Nanoparticles Incorporated into Silica Nanoreactors for Enhanced Hydrogenations, Angew. Chem. Int. Ed., 2019, 58, 14483–14488.

[6] M. Guo, X. Kong, Hydrogenation of benzoic acid derivatives over Pt/ TiO2 under mild conditions, Commun. Chem., 2021, 4, 54.

[7] M. Wang, M. Guo, The Influence of Surface Structure of RhPt Bimetallic Nanoparticles on the Hydrogenation of Aromatic Compounds, J. Pys. Chem. C, 2021, 125, 15275–15282.

[8] H. Zhang, G. Li, One-pot synthesized mesoporous C-TiO_2 hybrid for Ru-catalyzed low-temperature hydrogenation of benzoic acid, J. Mater. Sci., 2019, 54, 7529–7540.

[9] Z. Jiang, G. Lan, Solid state synthesis of Ru–MC with highly dispersed semi-embedded ruthenium nanoparticles in a porous carbon framework for benzoic acid hydrogenation, Catal. Sci. Technol., 2016, 6, 7259.

[10] X. Xu, M. Tang, Hydrogenation of Benzoic Acid and Derivatives over Pd

Nanoparticles Supported on N-Doped Carbon Derived from Glucosamine Hydrochloride, ACS Catal., 2014, 4, 3132−3135.

[11] C. Chaudhari, H. Imatome, Recyclable Rh-PVP nanoparticles catalyzed hydrogenation of benzoic acid derivatives and quinolines under solvent-free conditions, Catal. Commun., 2019, 126, 55–60.

[12] H. Zhang, J. Dong, In-situ generated highly dispersed nickel nanoclusters confined in MgAl mixed metal oxide platelets for benzoic acid hydrogenation, J. Catal., 2019, 372, 258–265.

[13] X.H. Lu, Y. Shen, Selective hydrogenation of benzoic acid to cyclohexane carboxylic acid over microwave-activated Ni/carbon catalysts, Mol. Catal., 2018, 444, 53–61.

[14] M. Liu, C. Wang, Coral-shaped PtRu/$Ni(OH)_2$ electrocatalyst promotes selective hydrogenation of benzoic acid, Catal. Sci. Technol., 2023, 13, 3568–3578.

[15] A. Fukazawa, Y. Shimizu, Electrocatalytic hydrogenation of benzoic acids in a proton-exchange membrane reactor, Org. Biomol. Chem., 2021, 19, 7363.

[16] Y. Du, X. Chen, Electrocatalysis as an Efficient Alternative to Thermal Catalysis over PtRu Bimetallic Catalysts for Hydrogenation of Benzoic Acid Derivatives, Green Chem., 2023, 25, 5489–5500.